

Dual-wavelength polarization-tunable holographic response in an azobenzene-containing film

Hong Chen(陈红), Pan Wang(王潘), Ziyao Lyu(吕子瑶), and Changshun Wang(王长顺)
Citation: Chin. Phys. B, 2026, 35 (**5**): 054206. DOI: 10.1088/1674-1056/ae0b39
http://cpb.iphy.ac.cn; http://iopscience.iop.org/cpb

What follows is a list of articles you may be interested in

Synchronized dual-wavelength mode-locked laser in normal dispersion regime

Yangrui Shi(史洋瑞), Haojing Zhang(张皓景), Yuxuan Ren(任俞宣), Junsong Peng(彭俊松), and Heping Zeng(曾和平)
Chin. Phys. B, 2025, 34 (**9**): 094207. DOI: 10.1088/1674-1056/add4fe

Multi-wavelength and transversely mode-switchable fiber laser based on ring-core fiber Bragg grating

Ya-Jun Jiang(姜亚军), Yu-Hui Su(苏宇辉), Jia-Xin Gao(高嘉欣), Feng Zhou(周峰), Li-Qin Cheng(程丽琴), Kang-Wei Pan(潘康伟), Bin-Chuan Sun(孙镔传), Li Shen(申力), De-Xing Yang(杨德兴), and Jian-Lin Zhao(赵建林)
Chin. Phys. B, 2025, 34 (**6**): 064203. DOI: 10.1088/1674-1056/adc663

Yb:CaF_2–YF_3 transparent ceramics ultrafast laser at dual gain lines

Xiao-Qin Liu(刘晓琴), Qian-Qian Hao(郝倩倩), Jie Liu(刘杰), Dan-Hua Liu(刘丹华), Wei-Wei Li(李威威), and Liang-Bi Su(苏良碧)
Chin. Phys. B, 2022, 31 (**11**): 114205. DOI: 10.1088/1674-1056/ac720f

Possibility to break through limitation of measurement range in dual-wavelength digital holography

Tuo Li(李拓), Wen-Xiu Lei(雷文秀), Xin-Kai Sun(孙鑫凯), Jun Dong(董军), Ye Tao(陶冶), and Yi-Shi Shi(史祎诗)
Chin. Phys. B, 2021, 30 (**9**): 094201. DOI: 10.1088/1674-1056/abf348

Pulse generation of erbium-doped fiber laser based on liquid-exfoliated $FePS_3$

Qing Yin(阴晴), Jin Wang(汪进), Xin-Yao Shi(史鑫尧), Tao Wang(王涛), Jie Yang(杨洁), Xin-Xin Zhao(赵新新), Zhen-Jiang Shen(沈振江), Jian Wu(吴坚), Kai Zhang(张凯), Pu Zhou(周朴), Zong-Fu Jiang(姜宗福)
Chin. Phys. B, 2019, 28 (**8**): 084208. DOI: 10.1088/1674-1056/28/8/084208

Dual-wavelength polarization-tunable holographic response in an azobenzene-containing film

Hong Chen(陈红)[1], Pan Wang(王潘)[2], Ziyao Lyu(吕子瑶)[3], and Changshun Wang(王长顺)[1,†]

[1] *State Key Laboratory of Advanced Optical Communication Systems and Networks, School of Physics and Astronomy, Shanghai Jiao Tong University, Shanghai* 200240, *China*

[2] *Department of Information and Communications Engineering, Institute of Science Tokyo, Tokyo* 1528550, *Japan*

[3] *State Key Laboratory of Space-Ground Integrated Information Technology, Beijing Institute of Satellite Information Engineering, Beijing* 100095, *China*

(Received 29 July 2025; revised manuscript received 9 September 2025; accepted manuscript online 25 September 2025)

We report a polarization-tunable holographic system in an azobenzene-containing liquid crystal film enabled by dual-wavelength excitation. The 405-nm beam facilitates the accumulation of cis-isomers and enhances molecular mobility, while the 532-nm beams induce photoisomerization and polarization-selective molecular alignment. Their cooperative action yields a nonlinear holographic response, resulting in a twofold increase in diffraction efficiency compared to single-wavelength excitation. By tuning the polarization states of the 532-nm beams, a continuous transition from an amplitude to polarization grating is realized, together with passive all-optical switching. This approach offers a versatile strategy for dynamic holographic modulation, with potential applications in tunable photonic elements, polarization-selective optical devices, and reconfigurable optical switches driven by polarization control.

Keywords: dual-wavelength, polarization-tunable, azobenzene

PACS: 42.15.–i, 42.25.–p, 42.25.Hz, 42.25.Ja

DOI: 10.1088/1674-1056/ae0b39 **CSTR:** 32038.14.CPB.ae0b39

1. Introduction

Conventional electronic computing faces energy and speed limitations, hindering progress in advanced information technologies.[1] In contrast, optical computing[2–4] has attracted significant attention due to its inherent advantages, including high parallelism, low latency, strong resistance to electromagnetic interference, and ultra-low power consumption. The integration of photonic devices in data transmission, processing, and storage is widely viewed as a critical pathway to next-generation information processing systems.[5] Holography[6,7] has emerged as a compelling approach for functional optical computing, attributed to its unique capacity for spatial modulation, multidimensional information multiplexing, and high-density data storage.[8–10] By introducing the vectorial degree of freedom for information encoding,[11] polarization holography[12–14] enables high-dimensional control and significantly enhances information capacity, positioning it as a key focus in current research.

Azobenzene molecules, known for their strong light-induced isomerization, have been widely incorporated into liquid crystal systems,[15–18] yielding azobenzene-containing liquid crystals[19,20] that exhibit pronounced photoresponsivity and photoinduced anisotropy.[21–24] Upon irradiation with linearly polarized light of appropriate wavelengths, the azobenzene molecules undergo reversible trans-cis-trans isomerization, inducing molecular reorientation perpendicular to the incident polarization. The resulting anisotropic state is erasable via thermal treatment or exposure to circularly polarized light, enabling rewritable optical modulation.[25] Such anisotropic alignment has been employed, for example, to fabricate colorless birefringent polymer films.[26] Gelebart *et al*. further demonstrated that embedded azobenzene derivatives exhibiting rapid thermal relaxation can be incorporated into liquid crystal networks to develop photoactive polymer films capable of sustaining continuous, directional macroscopic deformation under uniform illumination.[27] These self-shadow-driven feedback systems offer new opportunities for light-responsive microsystem design. Moreover, polarization-sensitive holographic gratings can be inscribed in azobenzene liquid crystal films by controlling the polarization state of the writing beams, enabling the realization of tunable all-optical beam splitters with adjustable splitting ratios.[28] Such passive-response photonic elements are promising candidates for practical applications in optical switching and signal routing.

However, conventional holographic techniques based on single-wavelength coherent interference often lack the flexibility required for advanced optical modulation. To overcome this limitation, Lv *et al*. introduced a dual-wavelength recording approach[29,30] in azobenzene films using a 532-nm laser as the switching source and two non-absorbing 633-nm lasers.[31] Nevertheless, the reported maximum diffraction efficiency was limited to 11.97%, as both wavelengths fall within relatively weak absorption regions. Thus, we

†Corresponding author. E-mail: cswang@sjtu.edu.cn

© 2026 Chinese Physical Society and IOP Publishing Ltd. All rights, including for text and data mining, AI training, and similar technologies, are reserved.

propose a dual-wavelength synergistic holographic recording scheme that combines a pair of 532-nm coherent beams with an auxiliary 405-nm beam in azobenzene-based photoresponsive films. The 405-nm light, operating within the strong absorption band of azobenzene molecules, facilitates efficient trans–cis isomerization and enhances refractive index modulation in conjunction with the 532-nm beams. This synergistic interaction enables up to a twofold increase in diffraction efficiency relative to conventional schemes. Furthermore, by tailoring the polarization state of the 532-nm pump beam, the recorded grating can be tuned continuously from a phase grating to a polarization grating, enabling a passive, all-optical switching functionality. These results open new avenues for the development of polarization-controlled photonic components and all-optical logic elements.

2. Experimental setup

The experimental setup is illustrated in Fig. 1. A 532-nm laser (Nd:YAG laser, CW) was employed as the primary pump beam and split into two beams of equal intensity via a beam splitter. The polarization states of the two beams were independently controlled using polarizers (P_1, P_2) and half-wave plates (H_1, H_2), and both beams were directed to simultaneously illuminate the sample surface at an angle of 5°, enabling holographic recording. A 405-nm laser (Diode Laser, CW), incident normally, served as an auxiliary pump source. Its power was modulated using a variable optical attenuator (Att), and its illumination area was spatially overlapped with that of the 532-nm beams. A 633-nm laser (He–Ne laser, CW, 2 mW/cm^2) was used as the probe beam and was also normally incident onto the same region. The diffracted signal was monitored in real time using an oscilloscope (DPO 2022B Digital Phosphor Oscilloscope, Tektronix).

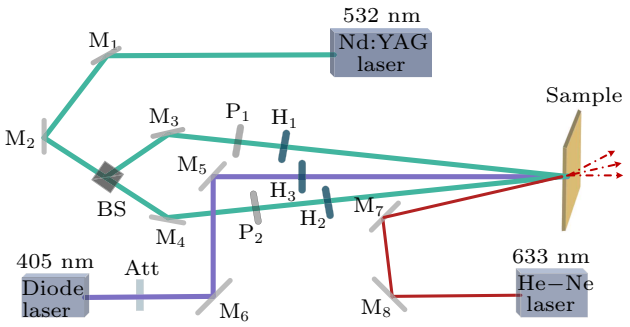


Fig. 1. Experimental setup for dual-wavelength polarization-tunable holographic response in an azobenzene-containing film. (M: mirror; P: polarizer; BS: beam splitter; H: half-wave plate; Att: attenuator. Sample: Azobenzene liquid crystal thin film).

The sample comprised a self-assembled azobenzene-containing liquid crystal film. It was prepared using Methyl Orange (MO, Sigma-Aldrich) and a poly(ionic liquid) (PIL, Sigma-Aldrich), by dropwise adding a 2-mg/ml aqueous solution of PIL to an equal-concentration MO solution at a 1:1 molar charge ratio. After precipitation and filtration, the complex was repeatedly washed with doubly distilled water to remove impurities, and then vacuum-dried at 60 °C for 12 hours. The final powder exhibited a melting point of ∼ 180 °C, with clear Schlieren textures observed upon cooling, reflecting its high orientational order. This film was confined between two glass substrates with a thickness of 10 μm and exhibited good structural uniformity. Both the 405-nm and 532-nm beams lie within the absorption band of the sample, whereas the 633-nm probe beam lies outside the absorption range.[32]

3. Results and discussion

A comparative experiment was initially carried out to examine the influence of the auxiliary 405-nm pump beam on the holographic recording process. Two coherent 532-nm beams (30 mW/cm^2, horizontal polarization) were employed in the absence of the 405-nm illumination. Their interference generated a spatially modulated intensity profile on the sample surface, which initiated trans–cis photoisomerization of azobenzene molecules and induced anisotropic molecular reorientation, leading to the formation of a refractive index modulation grating. The effect of introducing a 405-nm beam (20 mW/cm^2, horizontal polarization) in the presence of the two 532 nm writing beams was also examined. The diffraction efficiency was determined by the ratio of the diffracted power to the incident power of the 633-nm horizontally polarized probe beam.[28] The temporal evolution of diffraction efficiency under both conditions is presented in Fig. 2. In both cases, the diffraction efficiency displays a biphasic growth: a fast response followed by a slower process, which can be explained by photoinduced birefringence.[21,25] Initially, randomly oriented azobenzene molecules rapidly align perpendicular to the polarization of the incident light. As the side-chain reorientation proceeds, it gradually drives the reorganization of the liquid crystal main chains, slowing the overall reorientation rate. Unlike the 532-nm coherent beams that form an interference pattern, the 405-nm beam acts as a uniform excitation source. Its higher photon energy effectively promotes the trans–cis isomerization of azobenzene molecules. This significantly accelerates the photoisomerization kinetics and enhances molecular activation, facilitating the rapid development of anisotropic molecular alignment within the sample. Owing to its increased conformational flexibility and molecular mobility, the cis-isomer promotes localized structural relaxation, which in turn enhances the dynamic responsiveness of the film. This reduction in the reorientation energy barrier facilitates more efficient alignment of trans-isomers along the direction defined by the 532-nm interference field. As a result, the establishment of spatial anisotropy proceeds with greater rapidity, contributing to the nearly twice enhancement in diffraction efficiency observed under dual-wavelength illumination. This

cooperative mechanism effectively combines the spatial modulation capability of the 532-nm coherent beams with the dynamic molecular excitation induced by the 405-nm auxiliary beam, demonstrating a pronounced enhancement of photoinduced anisotropy.

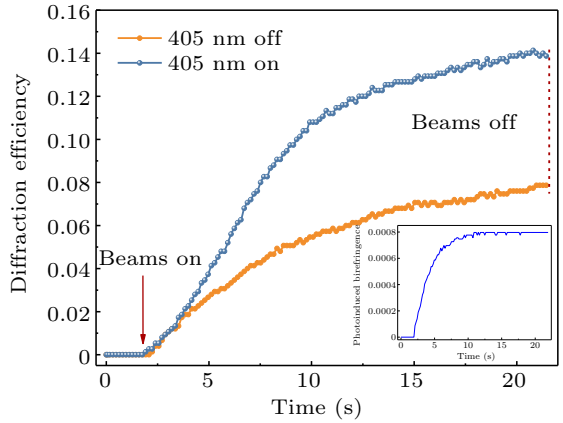


Fig. 2. Real-time diffraction efficiency with and without 405-nm light assistance. Inset: photoinduced birefringence in the absence of 405-nm light.

With both the 532-nm writing beams and the 405-nm auxiliary beam horizontally polarized, the real-time evolution of the diffracted power displayed a characteristic two-stage growth across different 405-nm intensities, as shown in Fig. 3. The maximum diffraction efficiency and the fastest initial growth rate were both observed at 60 mW/cm^2, demonstrating the optimal synergistic enhancement under this condition. At lower intensities (20 mW/cm^2 and 40 mW/cm^2), slower photoisomerization dynamics and reduced molecular reorientation efficiency were observed, attributed to the limited number of photoinduced molecules. In contrast, at 80 mW/cm^2, the formation of anisotropic structures was suppressed, which may be attributed to overaccumulation of cis-isomers.[33] These results suggest the existence of an optimal power window for the 405-nm auxiliary beam, where sufficient molecular activation is achieved without compromising the structural stability, thereby enabling enhanced diffraction efficiency.

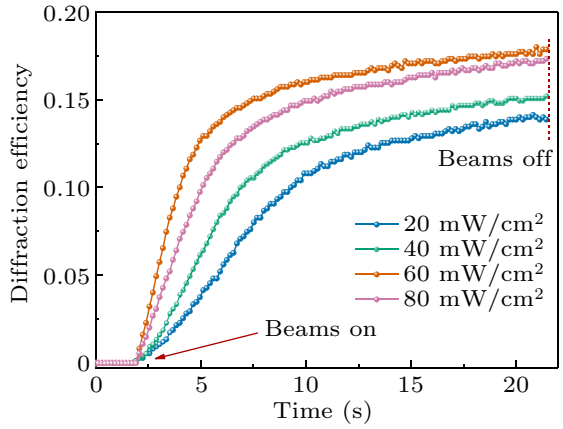


Fig. 3. Dual-wavelength holographic responses under varying 405-nm light power.

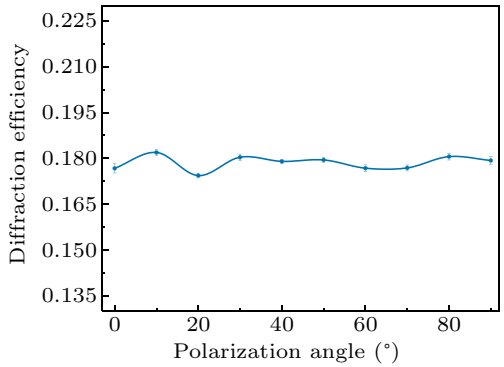


Fig. 4. Dual-wavelength holographic responses under varying 405-nm light polarization state.

The effect of the 405-nm auxiliary beam polarization on diffraction performance was further examined, with both 532-nm beams maintained at horizontal polarization. As shown in Fig. 4, the diffraction efficiency showed minimal dependence on the polarization state of the 405-nm beam. This behavior can be explained by the fact that the 405-nm auxiliary beam primarily excites the π–π^* band of azobenzene moieties, driving rapid trans–cis photoisomerization and leading to a quasi-randomized molecular orientation, rather than directly influencing polarization-dependent alignment.[34]

Different combinations of polarization state of the two 532-nm writing beams were employed to modulate the interference field structure and analyze their effect on the diffraction response, with the intensity of the 405-nm auxiliary beam fixed at 60 mW/cm^2 and that of the 532-nm beam at 30 mW/cm^2.[25] Parallel polarization of the two 532-nm beams produced an interference field characterized by a well-defined spatial intensity modulation within the sample.

$$E_{\parallel} = \begin{bmatrix} \sqrt{2}\cos\theta \\ 0 \end{bmatrix}. \tag{1}$$

Here, θ represents the optical phase. Periodic modulation of the refractive index in the azobenzene liquid crystal sample was established by the spatial intensity distribution, enabling the inscription of a phase grating.

$$T_{\parallel} = \begin{bmatrix} \exp\{i\Delta\varphi[1+\cos(2\theta)]\} & 0 \\ 0 & \exp\{-i\Delta\varphi[1+\cos(2\theta)]\} \end{bmatrix}, \tag{2}$$

where

$$\Delta\varphi = 2\pi\Delta n d/\lambda. \tag{3}$$

Here, Δn denotes the photoinduced refractive index, d is the sample thickness, and λ is the wavelength of the incident light.

Therefore, when the 633-nm probe beam is incident on the grating,

$$P = \begin{bmatrix} 1 \\ 0 \end{bmatrix}, \tag{4}$$

the diffraction efficiency is given by

$$\eta_{\parallel} = \Delta\varphi^2/4. \tag{5}$$

The real-time diffraction efficiency (dark blue dashed line in Fig. 5) stabilized at 17.86%, representing the highest value achieved. The parallel polarization combination was identified as the most effective in promoting anisotropic structure formation, resulting in a photoinduced birefringence Δn of 0.0071. As the angle between the two polarization directions increased, the diffraction efficiency gradually decreased, reaching a minimum under orthogonal polarization (inset of Fig. 5), at which point a polarization holographic grating was recorded

$$T_{\perp} = \begin{bmatrix} \exp[\mathrm{i}\Delta\varphi\cos(2\theta)] & 0 \\ 0 & \exp[-\mathrm{i}\Delta\varphi\cos(2\theta)] \end{bmatrix}. \quad (6)$$

The diffraction efficiency is given by

$$\eta_{\perp} = 4\mathrm{J}_1^2(\Delta\varphi). \quad (7)$$

Here, J_1 is the first-order Bessel function. As shown by the light blue dotted line in Fig. 5, the final diffraction efficiency stabilizes at 13.26%, with the corresponding photoinduced birefringence Δn calculated to 0.0078. The higher diffraction efficiency under parallel polarization results from optimal interference, while the larger birefringence under orthogonal polarization is due to enhanced molecular reorientation. When the polarization directions are between the two extreme cases, the recorded structure exhibits features of both phase and polarization gratings, implying the formation of a hybrid grating.

$$T = \begin{bmatrix} f_1\exp\{\mathrm{i}\Delta\varphi[1+\cos(2\theta)]\} + f_2\exp[\mathrm{i}\Delta\varphi\cos(2\theta)] & 0 \\ 0 & f_1\exp\{-\mathrm{i}\Delta\varphi[1+\cos(2\theta)]\} + f_2\exp[-\mathrm{i}\Delta\varphi\cos(2\theta)] \end{bmatrix}. \quad (8)$$

Here, f_1 and f_2 are the coupling factors associated with the polarization states. The formation of these gratings involves simultaneous phase and polarization modulation. Regardless of the specific modulation mechanism, the diffraction efficiency exhibits a double-exponential temporal behavior[35]

$$\eta = k_{\mathrm{f}}[1-\exp(-\beta_{\mathrm{f}}t)] + k_{\mathrm{s}}[1-\exp(-\beta_{\mathrm{s}}t)] + C. \quad (9)$$

Here, k_{f} and k_{s} are the pre-factors for the fast and slow processes, respectively, while β_{f} and β_{s} are the rate constants for these two processes, as fitted by the gray curves in Fig. 5. At a polarization angle difference of approximately 20°, the diffraction efficiency demonstrates maximum sensitivity, characterized by the most rapid response variation. This phenomenon results from the interplay between cooperative molecular orientation and perturbative competition mechanisms in the azobenzene medium. The strong dependence of grating formation on the polarization state can be attributed to the intrinsic sensitivity of azobenzene molecules to polarization-modulated interference fields.

To further explore the wavelength dependence of the cooperative recording mechanism, a modified writing configuration was employed in which 633 nm light replaced 532 nm as the primary writing wavelength, with 405-nm serving as the auxiliary pump. Both phase and polarization-sensitive holographic structures were targeted under this dual-wavelength exposure. However, no detectable holographic modulation was observed. The diffraction efficiency is primarily determined by the wavelength of the writing beam (532 nm). The 405-nm auxiliary beam enhances the process but cannot drive grating formation alone, whereas 633 nm, located outside the major absorption region of azobenzene, contributes negligibly to isomerization.

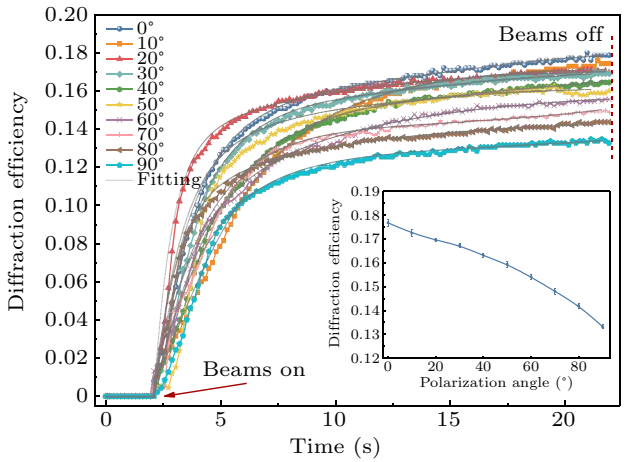


Fig. 5. Dual-wavelength holographic responses under varying 532-nm light polarization state.

Table. 1. Polarization-controlled optical switching based on dual-wavelength holographic writing.

Auxiliary pump beam	Pump beams	Probe beam	Diffraction beam	Logic state
↔	↔	↔	↔	**0**
	↔		↔	
↔	↔	↔	↕	**1**
	↕		↕	

By carefully tailoring the polarization configuration of the writing beams, binary modulation of the diffracted probe

beam polarization can be achieved. Specifically, parallel linear polarization of the 405-nm and 532-nm beams (both horizontal) induces a grating that preserves the polarization state of the 633-nm probe beam, corresponding to a logic state of "0" (Table 1). Conversely, mutually orthogonal polarization of the 532-nm beams produces a polarization grating that rotates the probe polarization to the vertical state, representing a logic state of "1". This polarization-encoded switching behavior demonstrates a reconfigurable output channel governed solely by the polarization states of the writing beams, serving as a fundamental mechanism for polarization-controlled optical switches and logic operations. The grating can be erased and rewritten by adjusting the light polarization, allowing multiple switching cycles without significant degradation.

4. Conclusion

In conclusion, a dual-wavelength-induced, polarization-tunable holographic recording system in an azobenzene-containing liquid crystal film has been demonstrated. The synergistic effect of the 405-nm auxiliary beam, which enhances molecular mobility, and the 532-nm pump beams, which drive anisotropic molecular alignment, results in a twofold enhancement in diffraction efficiency compared to single-wavelength excitation. By tailoring the polarization configuration of the pump beams, a continuous transition between phase and polarization gratings is achieved, allowing all-optical switching modulation of the polarization state of the diffracted beam. This work establishes a solid foundation for the development of efficient, reconfigurable holographic system and paves the way for a wide range of applications, including advanced photonic circuits, next-generation optical storage, quantum information processing, and dynamically reconfigurable optical networks. Further improvements, such as material optimization and beam parameter tuning, could help enhance performance for practical implementation in these areas.

Acknowledgement

Project supported by the National Natural Science Foundation of China (Grant Nos. 62475148 and 62505028).

References

[1] Moore G E 1998 *Proc. IEEE* **86** 82
[2] Northup T E and Blatt R 2014 *Nat. Photon.* **8** 356
[3] Solli D R and Jalali B 2015 *Nat. Photon.* **9** 704
[4] Wetzstein G, Ozcan A. Gigan S, Fan S, Englund D, Soljacic M, Denz C, Miller D A B and Psaltis D 2020 *Nature* **588** 39
[5] Lian C, Vagionas C, Alexoudi T, Pleros N, Youngblood N and Rios C 2022 *Nanophotonics* **11** 3823
[6] Wang L Zhou N and Sun B 2024 *Chin. Phys. B* **33** 050501
[7] Tian Y, Wu X N and Zhang H 2023 *Chin. Phys. Lett.* **40** 100402
[8] Huang Z Z and Cao L C 2024 *Light Sci. Appl.* **13** 43
[9] Ouyang W Q, Xu X Y, Lu W P, Zhao N, Han F and Chen S C 2023 *Nat. Commun.* **14** 9
[10] Shi L, Li B C, Kim C, Kellnhofer P and Matusik W 2021 *Nature* **591** 234
[11] Lyu Z, Dong T, Du Y J, Chen H and Wang C S 2025 *Laser Photon. Rev.* **19** 2402197
[12] Zhao R, Sain B, Wei Q, Tang C, Li X, Weiss T, Huang L, Wang Y and Zentgraf T 2018 *Light Sci. Appl.* **7** 95
[13] Genevet P and Capasso F 2015 *Rep. Prog. Phys.* **78** 024401
[14] Kim I, Jang J, Kim G, Lee J, Badloe T, Mun J and Rho J 2021 *Nat. Commun.* **12** 3614
[15] Wang Y, Fan F and Zhao H 2025 *Opto-Electron. Adv.* **8** 240250
[16] Zhao H, Guo J and Fan F 2025 *Laser Photon. Rev.* **19** 2402084
[17] Wang Y M, Fan F and Zhao H J 2024 *Photon. Res.* **12** 2148
[18] Zhao H, Fan F and Wang Y 2024 *Laser Photon. Rev.* **18** 2400442
[19] Gorkhali S P, Cloutier S G, Crawford G P and Pelcovits R A 2006 *Appl. Phys. Lett.* **88** 251113
[20] Choi H, Woo J H, Wu J W, Kim D W, Lim T K and Song S H 2007 *Appl. Phys. Lett.* **91** 141112
[21] Chen H, Lyu Z and Wang C 2024 *Photon. Res.* **12** 749
[22] Pan S, Ni M, Mu B, Li Q, Hu X Y, Lin C, Chen D and Wang L 2015 *Adv. Funct. Mater.* **25** 3571
[23] Lyu Z, Wang P and Wang C 2023 *Chin. Phys. B* **32** 124209
[24] Zhang L, Liu H, Liu Y and Wu Z 2022 *Chem. Commun.* **58** 3811
[25] Chen H, Lyu Z and Wang C 2025 *Opt. Commun.* **583** 131717
[26] Bugakov M, Shibaev V and Boiko N 2025 *ChemPhysChem* **26** e202400677
[27] Gelebart A H, Mulder D J, Varga M, Konya A, Vantomme G, Meijer E W, Selinger R L B and Broer D J 2017 *Nature* **546** 632
[28] Lyu Z, Wang C, Pan Y, Xia R, Chen T and Sun L 2019 *Opt. Lett.* **44** 2129
[29] Yeh H C, Chen G H and Lee C R 2007 *Appl. Phys. Lett.* **90** 181921
[30] Lin H C, Chu C W and Li M S 2011 *Opt. Express* **19** 13118
[31] Lyu Z, Wang C, Li H, Pan Y and Xia R 2018 *Opt. Mater. Express* **8** 2050
[32] Lyu Z and Wang C S 2022 *Front. Phys.* **10**
[33] Kozanecka S A, Switkowski K and Schab B E 2015 *Appl. Phys. B* **119** 227
[34] Merritt I C D, Jacquemin D and Vacher M 2021 *Phys. Chem. Chem. Phys.* **23** 19155
[35] Ho M S, Natansohn A and Rochon P 1995 *Macromolecules* **28** 6124